Continuum Mech. Thermodyn. (2012) 24:377–390
DOI 10.1007/s00161-012-0244-y

ORIGINAL ARTICLE

B. E. Abali · C. Völlmecke · B. Woodward · M. Kashtalyan · I. Guz · W. H. Müller

Numerical modeling of functionally graded materials using a variational formulation

Dedicated to Prof. Ingo Müller on the occasion of his 75th birthday

Received: 23 September 2011 / Accepted: 19 April 2012 / Published online: 12 May 2012

Abstract An approach of numerical modeling of heterogeneous, functionally graded materials, by using the finite element method, is proposed. The variational formulation is derived from the generic case so that the implementation of material coefficients, which are functions in space, is realized without any further assumptions. An analytical solution for a simple case is presented and used for validation of the numerical model.

Keywords Functionally graded materials · Variational formulation · Finite element method · Heterogeneous materials

1 Introduction

Functionally graded materials (FGMs) have recently emerged as the new class of advanced composite materials that show a gradual compositional variation of the constituents (e.g., metallic and ceramic) from one surface of the material to the other resulting in continuously varying material properties [16]. The gradual variation of material properties in FGMs is known to improve structural integrity and performance while preserving the intended thermal, tribological, and/or structural benefits of the constituent materials. FGMs were initially developed for super-heat-resistant materials to be used in aeronautics or nuclear technology. Now, the FGM concept is being widely explored in a variety of engineering applications including functional materials for sensors and thermogenerators [17], dental and orthopedic implants [20], and wear resistant coatings [24]. FGMs can also be used for joining dissimilar materials [25].

Although FGMs are highly heterogeneous materials, it is useful to idealize them as continua with properties that change smoothly with respect to spatial coordinates. A comprehensive review of principal developments in modeling and analysis of FGMs and structures is given by Birman and Byrd [3] covering homogenization of particulate FGMs, heat transfer issues, statics, dynamics, stability, fracture, testing, manufacturing, and design.

As the use of FGMs increases, new methodologies have to be developed to analyze and design structural components made of them. The main issue encountered in application of the finite element method to FGMs is how to model a material with continuously varying properties. The simplest approach involves the use of homogeneous elements each with different properties, giving a stepwise change in properties in the direction of the material gradient. This approach has already been used by several researchers and can give reasonably

Communicated by Stefan Seelecke.

B. E. Abali (✉) · C. Völlmecke · W. H. Müller
School V, Institute of Mechanics, Chair of Continuum Mechanics and Materials Theory,
Technical University of Berlin, Sekr. MS2, Einsteinufer 5, 10587 Berlin, Germany
E-mail: abali@tu-berlin.de

B. Woodward · M. Kashtalyan · I. Guz
School of Engineering, University of Aberdeen, Fraser Noble Building, Aberdeen AB24 3UE, Scotland, UK

accurate results. Etemadi et al. [6] modeled a sandwich panel with a functionally graded core subject to low-velocity impact. Zhang et al. [30] modeled the contact response of a functionally graded coating. Tilbrook et al. [26] and Wang and Nakamura [29] modeled the propagation of cracks in FGMs. There are, however, several problems in using this approach, which are discussed by Buttlar et al. [4]. Due to the model approximating the continually varying properties of the material with stepwise changes, a computational error is always introduced, particularly in cases of high stiffness gradients. In order to minimize this error, a very fine mesh in the direction of the property gradient is often required. This can, however, lead to extremely long computation times.

A more advanced method of including property variation into a finite element model is to use elements that themselves contain a gradient in properties. Santare and Lambros [23] proposed a 2-D graded element with material properties evaluated directly at the Gauss point. An alternative approach was adopted by Kim and Paulino [13], who have proposed a fully isoparametric element formulation that interpolates material properties at each Gauss point from the nodal values, using the same shape functions as the deformations. Comparisons of 2-D graded and homogenous elements under various loading conditions with analytical solutions in the literature showed that graded elements give far greater accuracy when modeling FGMs [13].

In this paper, the mathematical representation of the Galerkin finite element method is derived upon a variational formulation and position-dependent properties are directly integrated. Therefore, without any need of an element reformulation or reimplementation in the isoparametric space, the equations can be solved by using a various collection of novel algorithms from the FEniCS project [10], which are all released under open source GNU public license [7]. Moreover, a simple geometry and appropriate boundary conditions lead to an analytic solution that is used for verification of the approach. The advantage of that approach is that the material properties are approximated in the same functional space as the solution such that the same accuracy can be achieved.

At the beginning of the paper, the analytical solution is briefly outlined as derived in [11]. Then, starting with the variational formulation for the generic case, the specific problem, a simply supported plate under sinusoidal loading, is deduced. This allows to show the assumptions to be made and clarifies how the discretization of the material coefficients naturally arises. Subsequently, the numerical results are validated against the analytical solution, and parametric studies are presented. Having a verified finite element code will allow engineers to compute complex geometric structures with FGMs, and therefore, the code is presented under GNU public license in [1].

2 Problem statement

In order to determine the distribution of displacements u_i, in a linear elastic solid body, field equations of elasticity theory and boundary conditions are required. Without discussing their generality for the moment, we assume linear kinematic relations:

$$\varepsilon_{ij} = \frac{\partial u_{(i}}{\partial X_{j)}} = \frac{1}{2}\left(\frac{\partial u_i}{\partial X_j} + \frac{\partial u_j}{\partial X_i}\right), \tag{1}$$

equilibrium equations:

$$\frac{\partial \sigma_{ij}}{\partial X_j} = 0, \tag{2}$$

and a linear elastic constitutive Hooke's law for isotropic materials:

$$\sigma_{ij} = \frac{2G\nu}{1-2\nu}\varepsilon\delta_{ij} + 2G\varepsilon_{ij}, \tag{3}$$

where ε_{ij} are the components of the strain tensor, $\varepsilon = \frac{\partial u_i}{\partial X_i}$ is the volumetric strain or dilatation, σ_{ij} are the components of the stress tensor, and ν and G are Poisson's ratio and shear modulus, respectively. Einstein's summation convention is employed throughout. It should be pointed out that for FGMs, the material coefficients are no longer constants but functions of the material coordinate system $X_i = (X_1, X_2, X_3)$, and thus, material is heterogeneous. Here, the geometry is a plate with its thickness direction X_3. Since a variation of Poisson's ratio normally does not play a significant role in determining the magnitudes of stresses and displacements in FGMs, Poisson's ratio ν is commonly assumed to be constant, that is, $\nu = \text{const.}$ [22].

The shear modulus G is assumed to depend only on thickness, X_3. Even these simplified assumptions lead to a more complex problem than in the case of homogeneous materials.

Equations (1)–(3) form a set of 15 coupled partial differential equations for 15 unknowns. The number of field equations and unknowns can be reduced to three if the displacement formulation is used. For isotropic FGMs, the equilibrium equations in terms of displacements can be written as [19]:

$$\begin{aligned} G\Delta u_1 + \frac{G}{1-2\nu}\frac{\partial \varepsilon}{\partial X_1} + \left(\frac{\partial u_1}{\partial X_3} + \frac{\partial u_3}{\partial X_1}\right)\frac{\partial G}{\partial X_3} &= 0, \\ G\Delta u_2 + \frac{G}{1-2\nu}\frac{\partial \varepsilon}{\partial X_2} + \left(\frac{\partial u_2}{\partial X_3} + \frac{\partial u_3}{\partial X_2}\right)\frac{\partial G}{\partial X_3} &= 0, \\ G\Delta u_3 + \frac{G}{1-2\nu}\frac{\partial \varepsilon}{\partial X_3} + \varepsilon\frac{\mathrm{d}}{\mathrm{d}X_3}\left(\frac{2G\nu}{1-2\nu}\right) + 2\frac{\partial u_3}{\partial X_3}\frac{\mathrm{d}G}{\mathrm{d}X_3} &= 0, \end{aligned} \tag{4}$$

where $\Delta = \frac{\partial^2}{\partial X_1^2} + \frac{\partial^2}{\partial X_2^2} + \frac{\partial^2}{\partial X_3^2}$ denotes the Laplacian. For homogeneous materials, terms involving first-order derivatives of the material coefficients will vanish, and the equations, Eq. (4), will reduce to the well-known Navier- Lamé equations.

The system of Eq. (4) is still difficult to solve, and additional mathematical techniques have been developed for further simplification. One of the commonly used methods employs the use of displacement potential functions, which establish a representation for the displacements that automatically satisfies the equilibrium equations in terms of displacements. Equation (4) can be decoupled in terms of displacements [19] yielding to the following two equations for the displacement functions $L = L(X_1, X_2, X_3)$ and $N = N(X_1, X_2, X_3)$:

$$\Delta\left(\frac{1}{G}\Delta L\right) - \frac{1}{1-\nu}\left(\Delta - \frac{\partial^2}{\partial X_3^2}\right)L\frac{\mathrm{d}^2}{\mathrm{d}X_3^2}\left(\frac{1}{G}\right) = 0, \quad \Delta N + g(X_3)\frac{\partial N}{\partial X_3} = 0, \quad g(X_3) = \frac{\mathrm{d}}{\mathrm{d}X_3}\ln G(X_3). \tag{5}$$

The displacements can then be represented in terms of $L = L(X_i)$ and $N = N(X_i)$ as (cf., [19]):

$$\begin{aligned} u_1 &= -\frac{1}{2G}\left(\nu\Delta - \frac{\partial^2}{\partial X_3^2}\right)\frac{\partial L}{\partial X_1} + \frac{\partial N}{\partial X_2}, \\ u_2 &= -\frac{1}{2G}\left(\nu\Delta - \frac{\partial^2}{\partial X_3^2}\right)\frac{\partial L}{\partial X_2} - \frac{\partial N}{\partial X_1}, \\ u_3 &= -\frac{1}{G}\left(\nu\Delta - \frac{\partial^2}{\partial X_3^2}\right)\frac{\partial L}{\partial X_3} + \frac{\partial}{\partial X_3}\left[\frac{1}{2G}\left(\nu\Delta - \frac{\partial^2}{\partial X_3^2}\right)L\right]. \end{aligned} \tag{6}$$

By virtue of Hooke's law, Eq. (3), the stresses in an isotropic linearly elastic FGM with constant ν and thickness dependent $G(X_3)$ can be expressed in terms of displacement functions as follows:

$$\begin{aligned} \sigma_{11} &= \left(\nu\frac{\partial^2}{\partial X_2^2}\Delta + \frac{\partial^4}{\partial X_1^2\partial X_3^2}\right)L + 2G\frac{\partial^2 N}{\partial X_1\partial X_2}, \\ \sigma_{22} &= \left(\nu\frac{\partial^2}{\partial X_1^2}\Delta + \frac{\partial^4}{\partial X_2^2\partial X_3^2}\right)L - 2G\frac{\partial^2 N}{\partial X_1\partial X_2}, \\ \sigma_{33} &= \left(\Delta - \frac{\partial^2}{\partial X_3^2}\right)^2 L, \\ \sigma_{13} &= -\left(\Delta - \frac{\partial^2}{\partial X_3^2}\right)\frac{\partial^2 L}{\partial X_1\partial X_3} + G\frac{\partial^2 N}{\partial X_2\partial X_3}, \\ \sigma_{23} &= -\left(\Delta - \frac{\partial^2}{\partial X_3^2}\right)\frac{\partial^2 L}{\partial X_2\partial X_3} - G\frac{\partial^2 N}{\partial X_1\partial X_3}, \end{aligned} \tag{7}$$

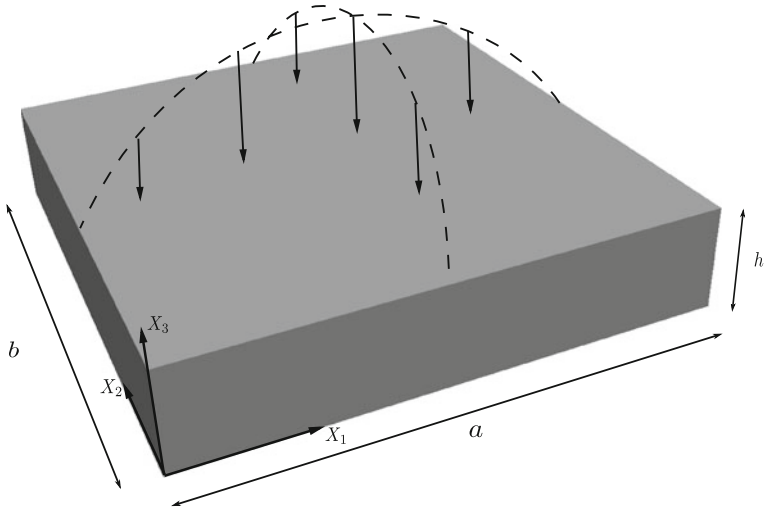

Fig. 1 Plate as a three-dimensional continuum under sinusoidal loading

$$\sigma_{12} = -\left(\nu\Delta - \frac{\partial^2}{\partial X_3^2}\right)\frac{\partial^2 L}{\partial X_1 \partial X_2} - G\left(\frac{\partial^2}{\partial X_1^2} - \frac{\partial^2}{\partial X_2^2}\right)N.$$

Plevako's displacement functions were recently revisited by Kashtalyan and Rushchitsky [12] who used a procedure similar to his and developed displacement functions for a transversely isotropic FGM.

Depending on the nature of the heterogeneity of the material and the boundary conditions on the surface of the solid, the solution of Eq. (4) or Eq. (5) could become quite complex, which limits the applicability of analytical methods. However, in some cases, it is still possible to generate an analytical solution for the 3-D elasticity boundary value problem for FGMs by using the displacement functions. One of these cases is a simply supported rectangular plate subjected to transverse loading, with exponential variation of the shear modulus through the thickness.

For this purpose, consider a plate of length a, width b, and thickness h, referred to a Cartesian coordinate system $X_i = (X_1, X_2, X_3)$ in material configuration so that $0 \leq X_1 \leq a$, $0 \leq X_2 \leq b$ and $0 \leq X_3 \leq h$ (Fig. 1). The material of the plate is a FGM with a constant Poisson's ratio ν and a shear modulus G varying exponentially through the thickness from G_0, the value at the bottom surface, to G_1, the value at the top surface, according to:

$$G(X_3) = G_1 \exp\left(\gamma\left(\frac{X_3}{h} - 1\right)\right), \quad \gamma = \ln\frac{G_1}{G_0}, \quad \nu = \text{const.}, \tag{8}$$

where γ is the inhomogeneity parameter. At the edges of the plate, Navier-type boundary conditions are assumed such that:

$$\begin{aligned}(X_1 = 0,\ X_2,\ X_3) \vee (X_1 = a,\ X_2,\ X_3): &\quad \sigma_{11} = 0,\ u_2 = u_3 = 0,\\ (X_1,\ X_2 = 0,\ X_3) \vee (X_1,\ X_2 = b,\ X_3): &\quad \sigma_{22} = 0,\ u_1 = u_3 = 0.\end{aligned} \tag{9}$$

The boundary conditions, Eq. (9), are representative of roller supports and analogous to simply supported edges used in plate theories. The top surface of the plate is subjected to transverse loading:

$$(X_1,\ X_2,\ X_3 = h): \quad \sigma_{33} = Q = -q \sin\frac{\pi m X_1}{a} \sin\frac{\pi m X_2}{b}, \quad \sigma_{31} = \sigma_{32} = 0, \tag{10}$$

where m and n are wave numbers, and q is the loading coefficient. The bottom surface of the plate is load-free, that is,

$$(X_1,\ X_2,\ X_3 = 0): \quad \sigma_{33} = \sigma_{32} = \sigma_{31} = 0. \tag{11}$$

An analytical solution to the above-stated boundary value problem was obtained in [9] by using the displacement functions method. It is presented in the Appendix for the sake of completeness.

3 Variational formulation

As outlined in the last section, an analytic solution can sometimes be obtained for a particular case of geometry, boundary, and loading conditions, specifically for a rectangular plate with simply supported edges and transverse sinusoidal loading as shown in Fig. 1. For practical purposes, other geometries and conditions are of interest, which may be approximated numerically. In this paper, the widely known finite element method (FEM), as an approximation in space, is implemented. We proceed to discuss its peculiarities in the present case.

Any function $\psi(\boldsymbol{X}, t)$, defined in space and time, is separated into a time-dependent and a space-dependent function:

$$\psi(\boldsymbol{X}, t) = \sum_{\mathrm{ID}} \Psi^{\mathrm{ID}}(t)\phi^{\mathrm{ID}}(\boldsymbol{X}). \tag{12}$$

This is undertaken for every nodal point with a unique identification number, ID. The space function $\phi^{\mathrm{ID}}(\boldsymbol{X})$ determines the connection of the nodal points; thus, it depends solely on the geometry. The time function $\Psi^{\mathrm{ID}}(t)$ represents the values of the function $\psi(\boldsymbol{X}, t)$ in each node. The value in each node has an influence in a finite domain, and thus, $\phi^{\mathrm{ID}}(\boldsymbol{X})$ has a local support. This local support, a functional space spanned over the affine connections $\{\phi^1, \phi^2, \ldots, \phi^{\text{node nr.}}\}$, is a HILBERT configuration $\mathcal{H}$ as defined in [9]. We choose to use linear space functions $\phi^{\mathrm{ID}}(\boldsymbol{X})$ so that the $\mathcal{H}$ configuration can be represented by a set of oblique axes. By choosing oblique axes, we need to distinguish between co- and contravariant notation, so that the contravariant components X^k of the absolute vector $\boldsymbol{X}$ are parallel projections to the axes.

The problem can appropriately be modeled as a closed system, which led us to choose material framework, that is, coordinates X^k label particles. The usual continuum mechanics notation (see [5,27] is applied. However, for simplicity, the configuration $\mathcal{H}$ will not be mentioned explicitly; thus, we write $\psi(X^k, t)$ while we mean $\underset{\mathcal{H}}{\psi}(X^k, t)$ for all the functions in that section.

A 3-D body in the known reference state $\mathcal{B}_0$ will be deformed under given loading conditions. The objective is to find the equation of the displacement field u_i which is the difference between the reference and the deformed state of the body, $\mathcal{B}_0$ and $\mathcal{B}$, respectively. Both are closed domains. Thus, particles are not permitted to accumulate nor disintegrate, and identifiable by the material coordinates X^i. The coordinates of the particles X^i are known in the reference frame, which is the undeformed body $\mathcal{B}_0$ itself. Furthermore, the displacements must not violate the conservation laws. Hence, we can start off the conservation laws and end up with the equations for which the analytical solution is found. The usual assumptions in linear elasticity theory allow to employ a heterogeneous material. In order to justify and in addition to assure that the formulation for the numerical approximation does not contradict these assumptions, we briefly review the origin of Eq. (2).

The balance of mass and linear momentum read in the deformed state:

$$\frac{\mathrm{d}}{\mathrm{d}t}\int_{\mathcal{B}} \rho \,\mathrm{d}V = 0, \quad \frac{\mathrm{d}}{\mathrm{d}t}\int_{\mathcal{B}} \rho v_i \,\mathrm{d}V = \int_{\partial\mathcal{B}} n^j \sigma_{ji} \,\mathrm{d}a + \int_{\mathcal{B}} \rho f_i \,\mathrm{d}V, \tag{13}$$

where the mass density ρ, velocities v_i, and body forces f_i are the numerical values of corresponding functions. Moreover, plane normal on the surface n^j and momentum flux σ_{ji}, given by the CAUCHY stress tensor, refer to the deformed state, $\mathcal{B}$. Of course, Eq. (13) can also be expressed in the reference state $\mathcal{B}_0$, to which the coordinates X^i refer. The sought displacements u^i are then the difference of the coordinates in the deformed state x^i and the coordinates in the undeformed, that is, reference, state X^i. The volume element $\mathrm{d}V$ in the deformed state $\mathcal{B}$ is related to the volume element $\mathrm{d}V_0$ in the undeformed state $\mathcal{B}_0$ by [18, p. 62]:

$$\mathrm{d}V = \det\left(\frac{\partial x_i}{\partial X^j}\right) \mathrm{d}V_0 = J \,\mathrm{d}V_0, \tag{14}$$

where J stands for Jacobian and measures the deviation of the configuration from the reference state. Analogously, the relation between the area element $\mathrm{d}A$ in $\mathcal{B}$ and the area element $\mathrm{d}A_0$ in $\mathcal{B}_0$ can be obtained as:

$$n^i \,\mathrm{d}a = \mathrm{d}a^i = \left(\frac{\partial x_i}{\partial X^r}\right)^{-1} J N_r \,\mathrm{d}A_0, \tag{15}$$

where N_r represents normals to the tangent plane on the surface in $\mathcal{B}_0$. Consequently, by substituting Eq. (14) and (15) into Eq. (13) and implementing the conservation of mass, such that $\rho_0 = \rho/J = \text{const.}|_t$ holds, the balance law for linear momentum can be rewritten in the material configuration $\mathcal{B}_0$ as follows:

$$\int_{\mathcal{B}_0} \rho_0 \frac{\partial v_i}{\partial t} \,\mathrm{d}V_0 = \int_{\partial\mathcal{B}_0} \sigma_{ji} \left(\frac{\partial x_j}{\partial X^r}\right)^{-1} J N_r \,\mathrm{d}A_0 + \int_{\mathcal{B}_0} \rho_0 f_i \,\mathrm{d}V_0. \tag{16}$$

Equation (16) holds in general for all closed systems. However, for our problem, firstly, the inertia term $\rho_0 \partial v_i/\partial t$ is neglected while the problem is assumed to be modeled accurately using stationarity. Secondly, the body forces f_i are ignored and deflection of the body under its own weight, caused by gravitation, is neglected. Subsequently, Eq. (16) reads as

$$0 = \int_{\partial\mathcal{B}_0} \sigma_{ji} \left(\frac{\partial x_j}{\partial X^r}\right)^{-1} J N_r \,\mathrm{d}A_0. \tag{17}$$

Analogously to the analytic solution, which stems from the static theory of linear elasticity, the assumption of small displacements is applied:

$$\frac{\partial x_j}{\partial X^r} \approx \delta_{jr}, \quad J = \det\left(\frac{\partial x_j}{\partial X^r}\right) \approx 1. \tag{18}$$

Moreover, continuity of stress within the body is assumed. Although the material is heterogeneous, it does not contain any singular surfaces. Hence, by applying the Gauss' theorem, the latter equation yields to the equilibrium condition (2) used in Sect. 2:

$$0 = \int_{\partial\mathcal{B}_0} \sigma^r{}_i N_r \,\mathrm{d}A_0 = \int_{\mathcal{B}_0} \frac{\partial \sigma^r{}_i}{\partial X^r} \,\mathrm{d}V_0 \Rightarrow \frac{\partial \sigma^r{}_i}{\partial X^r} = 0. \tag{19}$$

According to the Riesz representation theorem, any test function w^i of the same rank as the integrand (here a tensor of first order) can be chosen to contract the latter equation to an invariant under configuration transformation [21]:

$$0 = \int_{\mathcal{B}_0} \frac{\partial \sigma^r{}_i}{\partial X^r} w^i \,\mathrm{d}V_0, \tag{20}$$

such that it holds under deformed and undeformed states. Since the choice of the test functions is arbitrary, defining them as:

$$w^i = \sum_{\mathrm{ID}} 1^{\mathrm{ID}} \phi^{\mathrm{ID}}(X^i), \tag{21}$$

is admissible. This is also known as the Galerkin method. In order to integrate Eq. (20) in a discrete sense, Gauss quadrature is used:

$$\int_{\mathcal{B}_0} f \,\mathrm{d}V_0 = \sum_{i}^{n+1} f|_{p_i}\, g|_{p_i}, \quad f = \frac{\partial \sigma^r{}_i}{\partial X^r} w^i, \tag{22}$$

that is, we obtain a sum of products of the discrete function values $f|_{p_i}$ and weight function values $g|_{p_i}$ over $n+1$ tabulated integration points, p_i, which were first determined by Gauss and are known as Gauss points in the literature. They depend on the polynomial order n, which is determined by the element type. Here, we choose linear elements, and thus, two Gauss points in each direction are sufficient for a numerical integration.

However, calculating these points and their weights may be cumbersome. Since integration is additive, it can be evaluated in finite subdomains $\mathcal{B}_0^e$ and then summed up:

$$0 = \int_{\mathcal{B}_0} \frac{\partial \sigma^r{}_i}{\partial X^r} w^i \,\mathrm{d}V_0 = \bigcup_e \int_{\mathcal{B}_0^e} \frac{\partial \sigma^r{}_i}{\partial X^r} w^i \,\mathrm{d}V_0. \tag{23}$$

Every finite subdomain can be mapped into a geometrically identical subdomain (isoparametric element) upon which the GAUSS points and their weights are calculated and tabulated only once and where the integration according to Eq. (22) takes place. Hence, every function can be projected into discretized space and evaluated at the GAUSS points, which is a beneficial advantage when using the open source code FEniCS [14].

Traditionally, in conventional FEM software, the material coefficients are defined as constants per element. Therefore, modeling FGMs accurately is inevitably highly mesh dependent. Owing to the evaluation at the GAUSS points, utilizing FEniCS has the major advantage that any function can be evaluated in the same order of continuity in the discrete system as previously defined over the whole domain.

Equivalent to the formulation in the Sect. 2, linear symmetrical strains are introduced as follows:

$$\varepsilon^i{}_j = \frac{\partial u^{(i}}{\partial X^{j)}} = \frac{1}{2}\left(\frac{\partial u^i}{\partial X^j} + \frac{\partial u^j}{\partial X^i}\right) \tag{24}$$

and the constitutive relation is defined by HOOKE's law

$$\sigma^i{}_j = C^i{}_{jk}{}^l \varepsilon^k_l, \tag{25}$$

with an elasticity tensor of rank four. For the isotropic case, it can be described with two LAMÉ coefficients:

$$C^i{}_{jk}{}^l = \lambda \delta^i{}_j \delta_k{}^l + \mu(\delta^i{}_k \delta_j{}^l + \delta^{il}\delta_{jk}), \tag{26}$$

or with the widely known engineering material coefficients, YOUNG's modulus E, shear modulus G, and POISSON's ratio ν:

$$\lambda = \frac{E\nu}{(1+\nu)(1-2\nu)} = \frac{2G\nu}{(1-2\nu)}, \quad \mu = \frac{E}{2(1+\nu)} \equiv G. \tag{27}$$

Upon substitution of the kinematic and constitutive relation, the variational form in Eq. (23) can be rewritten in the interior of the domain, thus

$$0 = \int_{\mathcal{B}_0} \frac{\partial}{\partial X^r}\left(\frac{2G\nu}{(1-2\nu)}\delta^r{}_i \frac{\partial u^k}{\partial X^k} + 2G\frac{\partial u^{(r}}{\partial X^{i)}}\right) w^i \,\mathrm{d}V_0. \tag{28}$$

In general, boundary conditions are given in terms of the displacement on the boundary $\partial\mathcal{B}_D$ (DIRICHLET type) or in terms of the loading on the boundary $\partial\mathcal{B}_N$ (NEUMANN type):

$$\begin{aligned} u_i &= \bar{u}_i(X^k) = \hat{u}_i, \quad \forall X^k \in \partial\mathcal{B}_D, \\ N_r \sigma^r_i &= \frac{2G\nu}{(1-2\nu)} N_i \frac{\partial u^k}{\partial X^k} + 2GN_r \frac{\partial u^{(r}}{\partial X^{i)}} = t_i, \quad \forall X^k \in \partial\mathcal{B}_N, \end{aligned} \tag{29}$$

where $\partial\mathcal{B}_D \cap \partial\mathcal{B}_N = \{\}$ and $\partial\mathcal{B} = \partial\mathcal{B}_D \cup \partial\mathcal{B}_N$. The problem is well-defined if the conditions from Eq. (29)

$$\int_{\partial\mathcal{B}_D} (u_i - \hat{u}_i)\,\mathrm{d}A_0 = 0, \quad \int_{\partial\mathcal{B}_N} \left(N_r\sigma^r_i - t_i\right)\,\mathrm{d}A_0 = 0 \tag{30}$$

hold. By contracting with the same test functions (cf., Eq. (21)) and by adding these terms to Eq. (20), the following variational form results:

$$\int_{\partial\mathcal{B}_D} (u_i - \hat{u}_i) w^i \,\mathrm{d}A_0 + \int_{\partial\mathcal{B}_N} \left(N_r\sigma^r_i - t_i\right) w^i \,\mathrm{d}A_0 = \int_{\mathcal{B}_0} \frac{\partial \sigma^r_i}{\partial X^r} w^i \,\mathrm{d}V_0. \tag{31}$$

The chosen configuration $\mathcal{H}$ is linear in each finite element, and in other words, functions are allowed to be polynomials of degree one. Thus, the right side of Eq. (31), with the second order derivatives in u_i, cannot be adequately represented. This can be rectified by applying the GAUSS–OSTROGRADSKIY theorem (integration by parts for tensors):

$$\int_{\partial\mathcal{B}_D} (u_i - \hat{u}_i) w^i \,\mathrm{d}A_0 + \int_{\partial\mathcal{B}_N} (N_r\sigma^r_i - t_i) w^i \,\mathrm{d}A_0 = -\int_{\mathcal{B}_0} \sigma^r_i \frac{\partial w^i}{\partial X^r}\,\mathrm{d}V_0 + \int_{\partial\mathcal{B}} \sigma^r_i w^i N_r \,\mathrm{d}A_0, \tag{32}$$

since $\partial\mathcal{B} = \partial\mathcal{B}_D \cup \partial\mathcal{B}_N$, it follows:

$$\int\limits_{\partial\mathcal{B}_D} (u_i - \hat{u}_i - \sigma^r_i N_r) w^i \,\mathrm{d}A_0 - \int\limits_{\partial\mathcal{B}_N} t_i w^i \,\mathrm{d}A_0 = -\int\limits_{\mathcal{B}_0} \sigma^r_i \frac{\partial w^i}{\partial X^r} \,\mathrm{d}V_0. \tag{33}$$

By deriving Eq. (33), the coefficients were allowed to be functions in space. Finally, if test functions w^i are implemented such that they vanish on the DIRICHLET type boundaries, that is, $w^i\big|_{\partial\mathcal{B}_D} = 0$, and by using the same boundary conditions as in Eqs. (9), (10), (11), the variational form reads:

$$-\int\limits_{\partial\mathcal{B}_{\text{top}}} Q N_i w^i \,\mathrm{d}A_0 + \int\limits_{\mathcal{B}_0} \frac{2G\nu}{(1-2\nu)} \frac{\partial u^k}{\partial X^k} \frac{\partial w^i}{\partial X^i} \,\mathrm{d}V_0 + \int\limits_{\mathcal{B}_0} 2G \frac{\partial u^{(r}}{\partial X^{i)}} \frac{\partial w^i}{\partial X^r} \,\mathrm{d}V_0 = 0,$$
$$\partial\mathcal{B}_{\text{top}} = (X^1,\ X^2,\ X^3 = h). \tag{34}$$

This is the system of linear equations which has been programmed and solved by using the FEniCS project [14,10,15]. The visualization was undertaken with Paraview [8]. The code is supplied under GNU public license in [1].

4 Validation and results

In this section, the previously described numerical solution of the variational formulation is first tested for convergence. The model geometry is as explained in Sect. 2. The NEUMANN and DIRICHLET type boundaries as defined in Eqs. (9), (10), (11) are implemented. After the convergence test, results are presented for various values of the heterogeneity parameter γ (cf., $(8)_2$). According to γ, there is a neutral surface, along which exist zero displacements. The material is chosen to be heterogeneous only in the direction of thickness, that is, X^3. Therefore, the neutral surface is a plane, parallel to the X^1X^2 plane. If the parameter γ is set equal to zero, the neutral plane happens to be in the middle, as known from plate theory.

4.1 Convergence

As discussed in Sect. 3, employing the variational formulation in the numerical assessment allows the shear modulus to be defined as a function of position, that is, $G(X^i)$. Having applied the relevant boundary conditions, the variational form in Eq. (34) is well-posed and can be solved by using the finite element method. The solution is an approximation; thus, there is an discrepancy between the numerical solution and the analytical one, and the error depends on two choices. Firstly, it depends on the configuration, how the solution is discretized, that is, on the space functions $\phi^{\text{ID}}(X^k)$ in Eq. (12) which spans the HILBERT configuration $\mathcal{H}$, equipped with an L^2 norm [9]. Secondly, the error depends on the size of the finite elements, related to the size of the local support where the nodal value has influence. Since every function, including the material coefficient functions, is defined on the same configuration, the error of the approximation depends only on the size of the elements. Hence, if the error reduces globally, which is achieved by increasing the number of elements, the numerical approximation will converge to the analytical solution asymptotically.

In order to test the convergence, a box of $5 \times 5 \times 1$ m is modeled with the same number of elements in each direction, which is increased linearly from 10 to 50 in five steps. Material properties are chosen such that a nickel/alumina FGM [2] is realized with Al_2O_3 on top, $E_1 = 393.0\,\text{GPa}$, and Ni on bottom, $E_0 = 199.5\,\text{GPa}$, so that the inhomogeneity parameter γ and Poisson's ratio ν read:

$$\nu = 0.3,\quad \gamma = \ln\frac{G_1}{G_0} = \ln\frac{E_1}{E_0} = 0.6780,\quad G_1 = \frac{E_1}{2(1+\nu)}. \tag{35}$$

The convergence test for increasing degrees of freedom (DOF) can be seen in tabulated form in Table 1. The error is the discrepancy between the analytical (exact) u^{e}_i and numerical (approximate) u_i solution:

$$\text{err}_i = u^{\text{e}}_i - u_i. \tag{36}$$

Table 1 Results for the error in maximum norm, $\mathrm{err}_{\max}$, and density of the error in L^2 norm, err_{L^2}, stemming from the convergence analysis

No. of elements in each direction	Degrees of freedom	$\mathrm{err}_{\max}$	err_{L^2}
10	3, 993	0.389	12.252e−07
20	27, 783	0.128	3.998e−07
30	89, 373	0.066	1.937e−07
40	206, 763	0.042	1.161e−07
50	397, 953	0.031	0.792e−07

The values approach zero for increasing number of DOF

As the $\mathcal{H}$ configuration proposes the L^2 norm, its error has the size:

$$\|\mathrm{err}_i\|_{L^2} = \int_{\mathcal{B}_0} \mathrm{err}_i \; \mathrm{err}_i \, \mathrm{d}V_0. \tag{37}$$

However, this depends on the chosen volume. Therefore, the density of it is a more appropriate quantity to use for the convergence, that is,

$$\mathrm{err}_{L^2} = \frac{\|\mathrm{err}_i\|_{L^2}}{\int_{\mathcal{B}_0} \mathrm{d}V_0}. \tag{38}$$

Moreover, the quantity in L^2 norm has not a physical meaning. For practical purposes, it is more helpful to calculate the maximum of the error as follows:

$$\mathrm{err}_{\max} = \max \left(\mathrm{err}_i = u_i^{\mathrm{e}} - u_i \text{ in } \mathcal{B}_0 \right), \tag{39}$$

which is the maximum error existing in the whole body. By increasing the number of elements in the body, the position of the maximum error might change; thus, it does not measure the convergence. Hence, for the convergence, emphasis is put upon the error density in the L^2 norm.

Theoretically, once the error converges to zero, the numerical model is validated, since the finite element method has the analytical solution as its upper bound. Therefore, the model is validated against the analytical solution since the values in Table 1 clearly demonstrate the convergence of the model while the L^2 norm progresses toward zero. The quality of the accuracy, that is, the maximum of the error, depends on the problem specifications and can be improved by increasing the number of elements. Figure 2 shows the displacement, one component of the stress tensor and the VON MISES equivalent stress distribution of the body when using the realistic material properties from above and a lateral traction amplitude of $Q = 10\,\mathrm{MPa}$. The corresponding responses are as expected and manifest the reliability of the numerical results.

4.2 Results

In the previous paragraph, the convergence for 397953 DOF (cf., Table 1) has been demonstrated and validated. Further cases can now be investigated. In particular, the effects of changing values of the heterogeneity parameter γ will now be analyzed and discussed. In Table 2, the results of the numerical solution for the lateral deflection u_3 at the midpoint, that is, $(a/2, b/2, h/2)$, for varying values of γ from -2 to 2 are compared to the analytical solution u_3^{e} from Sect. 2. It can be noted that the relative error is sufficiently small for typical engineering applications, which demonstrates the accuracy of the model. Furthermore, it should be pointed out here that the relative error does not depend on the heterogeneity parameter γ. If γ tends toward zero, the material becomes homogeneous. Therefore, approaching the homogeneous solution from top and bottom sides, that is, by varying $\gamma > 0$ and $\gamma < 0$, sheds light on the versatility of the numerical model. The analytic solution for the homogeneous case has been proven and is well established [28].

Figure 3 illustrates the shift of the neutral plane for two different cases of the heterogeneity parameter, namely $\gamma = 0.1$ and $\gamma = 2.0$, Fig. 3a, b, respectively. Naturally, for $\gamma \to 0$, the neutral plane is at mid-height of the thickness, that is, at $X_3 = h/2$. As expected, when the heterogeneity γ is increased, the neutral plane moves toward the top of the plate owing to the implemented expression for γ (cf., Eq. $(8)_2$).

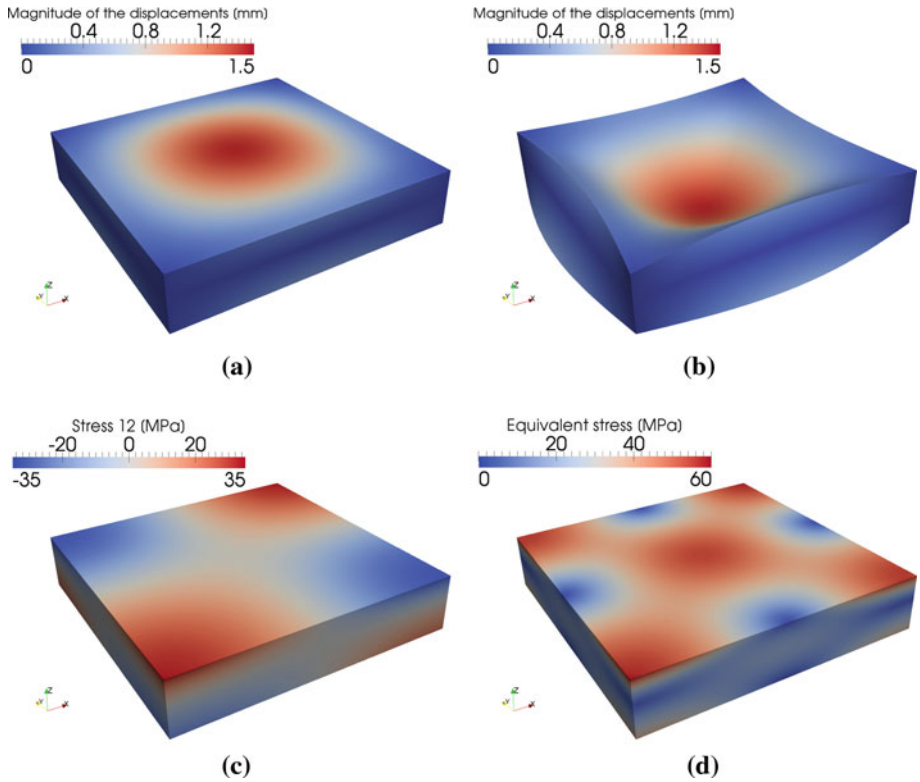

Fig. 2 Distribution of the magnitude of the displacement, **a** in deformed shape (1:1), **b** in deformed shape with scaled displacements for visualization (1:800). Distribution **c** of the stress component σ_{12} and **d** of the VON MISES equivalent stress

Table 2 Qualitative comparison of the results for the lateral deflection of the analytical u_3^{e} and numerical solutions u_3, at the midpoint $(a/2, b/2, h/2)$ of the geometry

γ	$\frac{G_1}{G_0} = \frac{E_1}{E_0}$	$u_3^{\mathrm{e}}(a/2, b/2, h/2)$	$u_3(a/2, b/2, h/2)$	Relative error
2.0	7.3891	−3.697	−3.680	0.0045
1.0	2.7183	−2.261	−2.235	0.0111
0.5	1.6487	−1.745	−1.731	0.0082
0.1	1.1052	−1.415	−1.406	0.0061
0.01	1.0101	−1.350	−1.341	0.0061
10^{-3}	1.0010	−1.343	−1.335	0.0061
10^{-4}	1.0001	−1.343	−1.335	0.0061
10^{-5}	1.0000	−1.343	−1.334	0.0061
-10^{-5}	1.0000	−1.343	−1.334	0.0061
-10^{-4}	0.9999	−1.343	−1.334	0.0061
-10^{-3}	0.9990	−1.342	−1.334	0.0061
−0.01	0.9901	−1.336	−1.328	0.0061
−0.1	0.9048	−1.274	−1.266	0.0062
−0.5	0.6065	−1.034	−1.025	0.0083
−1.0	0.3679	−0.794	−0.784	0.0118
−2.0	0.1353	−0.456	−0.455	0.0026

Additionally, the proposed formulation is compared to a *conventional* approach, where the function of shear modulus is approximated elementwise. This is achieved by choosing linear elements for the displacements again and zero order elements for the shear modulus, which is, therefore, constant in each element. No significant changes up to the third comma value in maximum error have been observed. Hence, for FGMs varying exponentially, an elementwise approximation appears to be acceptable from a numerical point of view. However, from the continuum mechanical point of view, this brings in another question about the continuity assumption of stress required in order to obtain the Eq. (19). On the other side, the computational time remains

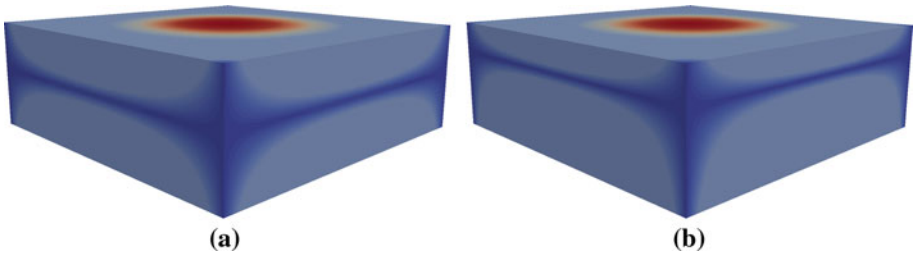

Fig. 3 Distribution of the magnitude of the displacement vector over $\mathcal{B}_0$ for two different heterogeneity parameters: **a** $\gamma = 0.1$ and **b** $\gamma = 2.0$. The neutral plane is moving away from the mid for increased inhomogeneity

the same, while both problems consist of the same number of degrees of freedom. Moreover, if one tries to compute the displacements with coefficients projected onto a lower order space than the displacements', then an additional convergence study is needed to show that the mesh is appropriate. Subsequently, by approximating the known material coefficient functions in the same space as the unknown displacement field, this cumbersome test becomes obsolete. Therefore, the approach proposed herein is more feasible.

5 Conclusions and outlook

An analytical solution of a simple geometry under sinusoidal loading with a functionally graded material was presented and a numerical solution to the same problem was applied and validated. For the generic case, starting from the balance equations, a variational form has been derived, programmed, and solved. The code is made public [1] for the sake of the open source community under GNU public license [7]. The numerical solution has been validated against the analytical solution. Even under variations of the heterogeneity parameter, a good accuracy has been obtained. This was possible by discretizing the material coefficient function and the displacement in the same configuration, so that the accuracy is the same for both and depends only on the size of the elements. The shown numerical approach is versatile and reliable, at least for smooth loading conditions. Having an analytical solution of a point loading would complete the verification of the numerical modeling and open the gate for complicated geometries modeling with FGMs. This is left to future research.

Acknowledgments The authors gratefully acknowledge funding by The Royal Society under grant number JP090633.

Appendix

First, the functions L and N in space $X_i = (x, y, z)$ are sought in the following form:

$$\begin{aligned} L(X_1, X_2, X_3) &= \psi_1(X_1, X_2)\phi_1(X_3), \\ N(X_1, X_2, X_3) &= \psi_2(X_1, X_2)\phi_2(X_3). \end{aligned} \tag{A1}$$

This leads to a transformation of Eq. (5) into the following four differential equations:

$$\begin{aligned} &\frac{\partial^2 \psi_i}{\partial X_1^2} + \frac{\partial^2 \psi_i}{\partial X_2^2} + \alpha^2 \psi_i = 0, \quad i = 1, 2, \\ &\frac{\mathrm{d}^4 \phi_1}{\mathrm{d}X_3^2} - 2g(X_3)\frac{\mathrm{d}^3 \phi_1}{\mathrm{d}X_3^3} + \left[g^2(X_3) - g'(X_3) - 2\alpha^2\right]\frac{\mathrm{d}^2 \phi_1}{\mathrm{d}X_3^2} + 2\alpha^2 g(X_3)\frac{\mathrm{d}\phi_1}{\mathrm{d}X_3} \\ &+ \alpha^2\left(\alpha^2 + \frac{\nu}{1-\nu}\left[g^2(X_3) - g'(X_3)\right]\right)\phi_1 = 0, \\ &\frac{\mathrm{d}^2 \phi_2}{\mathrm{d}X_3^2} + g(X_3)\frac{\mathrm{d}\phi_2}{\mathrm{d}X_3} - \alpha^2 \phi_2 = 0. \end{aligned} \tag{A2}$$

For a simply supported functionally graded rectangular plate with a dependence of the shear modulus on the thickness coordinate in the form $G(X_3) = G_1 \exp\left[\gamma\left(\frac{X_3}{h} - 1\right)\right]$, $G_1 = \text{const.}$, the functions ψ_1, ψ_2, ϕ_1, ϕ_2, in Eq. (A2), are given by:

$$
\begin{aligned}
\psi_1(X_1, X_2) &= \sin\frac{\pi m X_1}{a}\sin\frac{\pi n X_2}{b},\\
\psi_1(X_1, X_2) &= \cos\frac{\pi m X_1}{a}\cos\frac{\pi n X_2}{b},\\
\phi_1(X_3) &= qh^4\exp\frac{\gamma X_3}{h}\left(A_1\cosh\frac{\lambda X_3}{h}\cos\frac{\mu X_3}{h}+A_2\sinh\frac{\lambda X_3}{h}\cos\frac{\mu X_3}{h}\right.\\
&\quad\left.+A_3\cosh\frac{\lambda X_3}{h}\sin\frac{\mu X_3}{h}+A_4\sinh\frac{\lambda X_3}{h}\sin\frac{\mu X_3}{h}\right),\\
\phi_2(X_3) &= \frac{qh^2}{G_1}\exp\left(-\frac{\gamma X_3}{h}\right)\left(A_5\cosh\frac{\beta X_3}{h}+A_6\sinh\frac{\beta X_3}{h}\right),
\end{aligned}
\tag{A3}
$$

where

$$
\begin{pmatrix}\lambda\\ \mu\end{pmatrix} = \sqrt{\frac{1}{2}\left(\pm\beta^2+\sqrt{\beta^4+\gamma^2\alpha^2h^2\frac{\nu}{1-\nu}}\right)},\quad \beta=\sqrt{\frac{\gamma^2}{4}+\alpha^2h^2},\quad \alpha=\pi\sqrt{\left(\frac{m}{a}\right)^2+\left(\frac{n}{b}\right)^2}. \tag{A4}
$$

By substitution of the functions ψ_1, ψ_2, ϕ_1, ϕ_2, Eq. (A3) into Eq. A1), the following representation for displacements and stresses in the plate is obtained:

$$
\begin{aligned}
u_1 &= \sum_{k=1}^{6} A_k U_{1,k}(X_3)\cos\frac{\pi m X_1}{a}\sin\frac{\pi n X_2}{b},\\
u_2 &= \sum_{k=1}^{6} A_k U_{2,k}(X_3)\sin\frac{\pi m X_1}{a}\cos\frac{\pi n X_2}{b},\\
u_3 &= \sum_{k=1}^{6} A_k U_{3,k}(X_3)\sin\frac{\pi m X_1}{a}\sin\frac{\pi n X_2}{b},\\
\sigma_{jj} &= \sum_{k=1}^{6} A_k P_{jj,k}(X_3)\sin\frac{\pi m X_1}{a}\sin\frac{\pi n X_2}{b},\quad j=1,2,3,\\
\sigma_{13} &= \sum_{k=1}^{6} A_k P_{13,k}(X_3)\cos\frac{\pi m X_1}{a}\sin\frac{\pi n X_2}{b},\\
\sigma_{23} &= \sum_{k=1}^{6} A_k P_{23,k}(X_3)\sin\frac{\pi m X_1}{a}\sin\frac{\pi n X_2}{b},\\
\sigma_{12} &= \sum_{k=1}^{6} A_k P_{12,k}(X_3)\cos\frac{\pi m X_1}{a}\cos\frac{\pi n X_2}{b}.
\end{aligned}
\tag{A5}
$$

The constant coefficients A_k depend on the boundary conditions. The functions $U_{i,k}$ for the displacements:

$$
\begin{aligned}
U_{1,j}(\bar{X}_3) &= -\frac{qh}{2G_1}\frac{\pi mh}{a}\exp\left[-\gamma(\bar{X}_3-1)\right]\left[-\nu\alpha^2h^2f_j(\bar{x}_3)+(\nu-1)\frac{\mathrm{d}^2}{\mathrm{d}\bar{X}_3^2}f_j(\bar{X}_3)\right],\quad j=1,\ldots,4;\\
U_{1,j}(\bar{X}_3) &= -\frac{qh}{G_1}\frac{\pi nh}{b}f_j(\bar{X}_3),\quad j=5,6;\\
U_{2,j}(\bar{X}_3) &= -\frac{qh}{2G_1}\frac{\pi nh}{b}\exp\left[-\gamma(\bar{X}_3-1)\right]\left[-\nu\alpha^2h^2f_j(\bar{X}_3)+(\nu-1)\frac{\mathrm{d}^2}{\mathrm{d}\bar{X}_3^2}f_j(\bar{X}_3)\right],\quad j=1,\ldots,4;\\
U_{2,j}(\bar{X}_3) &= -\frac{qh}{G_1}\frac{\pi mh}{a}f_j(\bar{X}_3),\quad j=5,6;
\end{aligned}
\tag{A6}
$$

$$U_{3,j}(\bar{X}_3) = \frac{qh}{2G_1}\frac{\pi mh}{a}\exp\left[-\gamma(\bar{X}_3-1)\right]\left[(\nu-1)\left(-\gamma\frac{\mathrm{d}^2}{\mathrm{d}\bar{X}_3^2}f_j(\bar{X}_3)+\frac{\mathrm{d}^3}{\mathrm{d}\bar{X}_3^3}f_j(\bar{X}_3)\right)\right.$$
$$\left.-\alpha^2h^2\left((\nu-2)\frac{\mathrm{d}}{\mathrm{d}\bar{X}_3}f_j(\bar{X}_3)-\nu\gamma f_j(\bar{X}_3)\right)\right],\quad j=1,\ldots,4;$$
$$U_{3,j}(\bar{X}_3)=0,\quad j=5,6;$$

and the $P_{ij,k}$ for the stresses are found to be:

$$P_{11,j}(\bar{X}_3) = q\left[\nu\alpha^2h^2\left(\frac{\pi nh}{b}\right)^2 f_j(\bar{X}_3)-\nu\left(\frac{\pi nh}{b}\right)^2\frac{\mathrm{d}^2}{\mathrm{d}\bar{X}_3^2}f_j(\bar{X}_3)-\left(\frac{\pi mh}{a}\right)^2\frac{\mathrm{d}^2}{\mathrm{d}\bar{X}_3^2}f_j(\bar{X}_3)\right],$$
$$j=1,\ldots,4;$$
$$P_{11,j}(\bar{X}_3) = 2q\left(\frac{\pi mh}{a}\right)\left(\frac{\pi nh}{b}\right)\exp\left[\gamma\left(\bar{X}_3-1\right)\right]f_j(\bar{X}_3),\ j=5,6;$$
$$P_{22,j}(\bar{X}_3) = q\left[\nu\alpha^2h^2\left(\frac{\pi mh}{a}\right)^2 f_j(\bar{X}_3)-\nu\left(\frac{\pi mh}{a}\right)^2\frac{\mathrm{d}^2}{\mathrm{d}\bar{X}_3^2}f_j(\bar{X}_3)-\left(\frac{\pi nh}{b}\right)^2\frac{\mathrm{d}^2}{\mathrm{d}\bar{X}_3^2}f_j(\bar{X}_3)\right],$$
$$j=1,\ldots,4;$$
$$P_{22,j}(\bar{X}_3) = -2q\left(\frac{\pi mh}{a}\right)\left(\frac{\pi nh}{b}\right)\exp\left[\gamma\left(\bar{X}_3-1\right)\right]f_j(\bar{X}_3),\quad j=5,6;$$
$$P_{33,j}(\bar{X}_3) = q\alpha^4h^4f_j(\bar{X}_3),\quad j=1,\ldots,4;$$
$$P_{33,j}(\bar{X}_3) = 0,\quad j=5,6;\tag{A7}$$
$$P_{13,j}(\bar{X}_3) = q\alpha^2h^2\left(\frac{\pi mh}{a}\right)\frac{\mathrm{d}}{\mathrm{d}\bar{X}_3}f_j(\bar{X}_3),\quad j=1,\ldots,4;$$
$$P_{13,j}(\bar{X}_3) = -q\left(\frac{\pi nh}{b}\right)\exp\left[\gamma\left(\bar{X}_3-1\right)\right]f_j(\bar{X}_3),\quad j=5,6;$$
$$P_{23,j}(\bar{X}_3) = q\alpha^2h^2\left(\frac{\pi nh}{b}\right)\frac{\mathrm{d}}{\mathrm{d}\bar{X}_3}f_j(\bar{X}_3),\quad j=1,\ldots,4;$$
$$P_{23,j}(\bar{X}_3) = q\left(\frac{\pi mh}{a}\right)\exp\left[\gamma\left(\bar{X}_3-1\right)\right]f_j(\bar{X}_3),\quad j=5,6;$$
$$P_{12,j}(\bar{X}_3) = q\left(\frac{\pi mh}{a}\right)\left(\frac{\pi nh}{b}\right)\left[\nu\alpha^2h^2f_i(\bar{X}_3)+(1-\nu)\frac{\mathrm{d}^2}{\mathrm{d}\bar{X}_3^2}f_j(\bar{X}_3)\right],\quad j=1,\ldots,4;$$
$$P_{12,j}(\bar{X}_3) = q\left[\left(\frac{\pi mh}{a}\right)^2-\left(\frac{\pi nh}{b}\right)^2\right]\exp\left[\gamma\left(\bar{X}_3-1\right)\right]f_j(\bar{X}_3),\quad j=5,6.$$

In the expressions above, $\bar{X}_3 = X_3/h$, and functions $f_j(\bar{X}_3)$, $j=1,\ldots,6$ are:

$$f_1(\bar{X}_3)=\exp\left(\frac{\gamma\bar{X}_3}{2}\right)\cosh\lambda\bar{X}_3\cos\mu\bar{X}_3,\qquad f_2(\bar{X}_3)=\exp\left(\frac{\gamma\bar{X}_3}{2}\right)\sinh\lambda\bar{X}_3\cos\mu\bar{X}_3;$$
$$f_3(\bar{X}_3)=\exp\left(\frac{\gamma\bar{X}_3}{2}\right)\cosh\lambda\bar{X}_3\sin\mu\bar{X}_3,\qquad f_4(\bar{X}_3)=\exp\left(\frac{\gamma\bar{X}_3}{2}\right)\sinh\lambda\bar{X}_3\sin\mu\bar{X}_3;\tag{A8}$$
$$f_5(\bar{X}_3)=\exp\left(-\frac{\gamma\bar{X}_3L}{2}\right)\cosh\beta\bar{X}_3,\qquad f_6(\bar{X}_3)=\exp\left(-\frac{\gamma\bar{X}_3}{2}\right)\sinh\beta\bar{X}_3.$$

References

1. Abali, B.E.: Technical University of Berlin, Institute of Mechanics, Chair of Continuums Mechanics and Material Theory, Computational Reality. http://www.lkm.tu-berlin.de/ComputationalReality (2011)

2. Bhattacharyya, M., Kumar, A.N., Kapuria, S.: Synthesis and characterization of Al/SiC and Ni/Al203 functionally graded materials. Mater. Sci. Eng. A **487**, 524–535 (2008)
3. Birman, V., Byrd, L.W.: Modeling and analysis of functionally graded materials and structures. Appl. Mech. Rev. **60**(5), 195–216 (2007)
4. Buttlar, W.G., Paulino, G.H., Song, S.H.: Application of graded finite elements for asphalt pavements. J. Eng. Mech. **132**(3), 240–248 (2006)
5. Eringen, A.C.: Continuum Physics, Volume I, Mathematics. Academic Press, New York (1975)
6. Etemadi, E., Afaghi Khatibi, A., Takaffoli, M.: 3D finite element simulation of sandwich panels with a functionally graded core subjected to low velocity impact. Compos. Struct. **89**(1), 28–34 (2009)
7. Gnu Public: Gnu General Public License (2007). http://www.gnu.org/copyleft/gpl.html
8. Henderson, A.: ParaView Guide, a Parallel Visualization Application. Kitware Inc. http://paraview.org/
9. Hilbert, D.: (Transl. by Townsend E.J.): The Foundations of Geometry. The Open Court Publishing Co. (1902)
10. Hoffman, J., Jansson, J., Johnson, C., Knepley, M., Kirby, R., Logg, A., Scott, L.R., Wells, G.N.: Fenics (2005). http://www.fenicsproject.org/
11. Kashtalyan, M.: Three-dimensional elasticity solution for bending of functionally graded rectangular plates. Eur. J. Mech. A/Solids **23**(5), 853–864 (2004)
12. Kashtalyan, M., Rushchitsky, J.J.: Revisiting displacement functions in three-dimensional elasticity of inhomogeneous media. Int. J. Solids Struct. **46**(18–19), 3463–3470 (2009)
13. Kim, J.H.: Isoparametric graded finite elements for nonhomogeneous isotropic and orthotropic materials. J. Appl. Mech. **69**, 502–514 (2002)
14. Logg, A., Mardal, K.A., Wells, G.N.: Automated Solution of Differential Equations by the Finite Element Method, The FEniCS Book, Lecture Notes in Computational Science and Engineering, Vol. 84. Springer, UK (2011)
15. Logg, A., Wells, G.N.: Dolfin: automated finite element computing. ACM Trans. Math. Softw. **37**(2), 20:1–20:28 (2010). http://www.dspace.cam.ac.uk/handle/1810/221918/
16. Miyamoto, Y.: Functionally Graded Materials: Design, Processing, and Applications. Kluwer Academic Publishers, Boston (1999)
17. Müller, E., Dravsar, V.C., Schilz, J., Kaysser, W.: Functionally graded materials for sensor and energy applications. Mater. Sci. Eng. A **362**(1), 17–39 (2003)
18. Müller, W.H.: Streifzüge durch die Kontinuumstheorie. Springer, Berlin (2011)
19. Plevako, V.P.: On the theory of elasticity of inhomogeneous media. J. Appl. Math. Mech. **35**, 806–881 (1971)
20. Pompe, W., Worch, H., Epple, M., Friess, W., Gelinsky, M., Greil, P., Hempel, U., Scharnweber, D., Schulte, K.: Functionally graded materials for biomedical applications. Mater. Sci. Eng. A **362**(1–2), 40–60 (2003)
21. Rektorys, K.: Variational Methods in Mathematics, Science and Engineering. D. Reidel, Dordrecht in co-edit. with SNTL Prague (1975)
22. Sadd, M.H.: Elasticity: Theory, Applications, and Numerics. 2nd edn. Academic Press/Elsevier, Oxford/Amsterdam (2009)
23. Santare, M.H., Lambros, J.: Use of graded finite elements to model the behavior of nonhomogeneous materials. J. Appl. Mech. **67**(4), 819–822 (2000)
24. Schulz, U., Peters, M., Bach, F.W., Tegeder, G.: Graded coatings for thermal, wear and corrosion barriers. Mater. Sci. Eng. A **362**(1–2), 61–80 (2003)
25. Suresh, S., Mortensen, A.: Fundamentals of Functionally Graded Materials. Maney Publishing, London (1998)
26. Tilbrook, M.T., Moon, R.J., Hoffman, M.: Finite element simulations of crack propagation in functionally graded materials under flexural loading. Eng. Fract. Mech. **72**(16), 2444–2467 (2005)
27. Truesdell, C., Toupin, R.A.: Handbuch der Physik B and III/1, The Classical Field Theories. Springer, Edited by Flügge S (1960)
28. Vlasov, B.F.: On one case of bending of rectangular thick plate. Vestnik Moskov. Univ. Ser. Mat. Mekh. Astronom. Fiz. Khim. 25–34 (1957)
29. Wang, Z., Nakamura, T.: Simulations of crack propagation in elastic–plastic graded materials. Mech. Mater. **36**(7), 601–622 (2004)
30. Zhang, X.C., Xu, B.S., Wang, H.D., Wu, Y.X., Jiang, Y.: Hertzian contact response of single-layer, functionally graded and sandwich coatings. Mater. Des. **28**(1), 47–54 (2007)